Research Paper

Genetic characterization of a novel organoid from human malignant giant-cell tumor

Rie Suzuki [a,b,1], Toru Wakamatsu [a,b,1,*], Keiichi Yoshida [c], Yukiko Matsuoka [c],
Haruna Takami [a,b], Sho Nakai [a,b], Hironari Tamiya [a,b], Shigeki Kakunaga [a,b], Toshinari Yagi [a],
Ken-ichi Yoshida [d], Yoshinori Imura [b], Yoshihiro Yui [e], Satoru Sasagawa [f], Satoshi Takenaka [a,b]

[a] *Department of Musculoskeletal Oncology Service, Osaka International Cancer Institute, 3-1-69 Otemae, Chuo-ku, Osaka 541-8567, Japan*
[b] *Department of Orthopedic Surgery, Osaka University Graduate School of Medicine, 2-2 Yamadaoka, Suita, Osaka 565-0871, Japan*
[c] *Next-generation Precision Medicine Research Center, Osaka International Cancer Institute, 3-1-69 Otemae, Chuo-ku, Osaka 541-8567, Japan*
[d] *Department of Diagnostic Pathology and Cytology, Osaka International Cancer Institute, 3-1-69 Otemae, Chuo-ku, Osaka 541-8567, Japan*
[e] *Sarcoma Treatment Laboratory, Research Institute, Nozaki Tokushukai Hospital, Tanigawa 2-10-50, Daito, Osaka 574-0074, Japan*
[f] *Molecular Biology Laboratory, Research Institute, Nozaki Tokushukai Hospital, Tanigawa 2-10-50, Daito, Osaka 574-0074, Japan*

HIGHLIGHTS

- We investigated the genomic characteristics of our established novel organoids from human MGCTs.
- Our novel organoid model was genetically confirmed to be a malignant transformed tumor.
- Our organoid model could be used to elucidate the molecular pathogenesis of a MGCT and develop novel treatment modalities.

ARTICLE INFO

ABSTRACT

Malignant giant-cell tumors are extremely rare bone sarcomas that transform from conventional giant-cell tumors during long periods of treatment. Owing to their rarity, no further analysis of their molecular pathogenesis exists, and thus, no standard treatment has been established. Recently, organoid culture methods have been highlighted for recapturing the tumor microenvironment, and we have applied the culture methods and succeeded in establishing patient-derived organoids (PDO) of rare sarcomas. This study aimed to investigate the genomic characteristics of our established novel organoids from human malignant giant-cell tumors. At our institute, we treated a patient with malignant giant-cell tumor. The remaining sarcoma specimens after surgical resection were cultured according to the air–liquid interface organoid-culture method. Organoids were xenografted into NOD-scid IL2Rgnull mice. The developed tumors were histologically and genomically analyzed to compare their characteristics with those of the original tumors. Genetic changes over time throughout treatment were analyzed, and the genomic status of the established organoid was confirmed. Organoids from malignant giant-cell tumors could be serially maintained using air–liquid interface organoid-culture methods. The tumors developed in xenografted NOD-scid IL2Rgnull mice. After several repetitions of the process, a patient-derived organoid line from the malignant giant-cell tumor was established. Immunohistochemical analyses and next-generation sequencing revealed that the established organoids lacked the *H3-3A* G34W mutation. The xenografted organoids of the malignant giant-cell tumor had phenotypes histologically and genetically similar to those of the original tumor. The established organoids were confirmed to be derived from human malignant giant-cell tumors. In summary, the present study demonstrated a novel organoid model of a malignant giant-cell tumor that was genetically confirmed to be a malignant transformed tumor. Our organoid model could be used to elucidate the molecular pathogenesis of a malignant giant-cell tumor and develop novel treatment modalities.

---

* Corresponding author at: Department of Musculoskeletal Oncology Service, Osaka International Cancer Institute, 3-1-69 Otemae, Chuo-ku, Osaka 541-8567, Japan.
E-mail address: evolutionhhh49@yahoo.co.jp (T. Wakamatsu).
[1] Rie Suzuki and Toru Wakamatsu are equal contributors to this work and have been designated as co-first authors.

1. Introduction

Giant-cell tumor of the bone (GCTB) comprises 5% of all primary bone tumors [1–3]. Although GCTB shows local aggressiveness, it rarely metastasizes to the lungs [4]. Malignant giant-cell tumor (MGCT) is defined as a malignancy occurring from a GCTB with malignant transformation [5–7]. MGCTs can be primary (i.e., those consisting of conventional GCTB and sarcoma components at presentation) or secondary (i.e., those that occur subsequent to conventional GCTB), and most MGCTs are secondary [5,6]. Malignant transformation in GCTB is rare, occurring only in 2–9% of patients within ≥ 5 years [7–10]. It is unclear whether such malignant transformation is caused by repeated surgery, radiation, or denosumab, an anti-receptor activator of nuclear factor-kappa B ligand (RANKL) human monoclonal antibody [11–14].

Although the standard treatment for GCTB is surgical resection with bone curettage or resection, no standard or effective treatment for MGCT has been identified [6,10,12]. MGCTs typically present as high-grade tumors and histologically appear as undifferentiated pleomorphic sarcoma, osteosarcoma, or fibrosarcoma; thus, perioperative chemotherapy is often administered. Particularly, regimens for osteosarcoma, in combination with surgical resection with wide margins, are used for MGCTs demonstrating an osteosarcoma phenotype. However, the efficacy of these regimens is still unclear, and patients have poor prognoses [10]. Novel treatment modalities for MGCT based on its molecular pathogenesis and sarcoma mechanisms are required to improve prognosis.

Genetically, over 90% of GCTB cases have characteristic point mutations at the G34 position of *H3-3A*, encoding histone H3.3, leading to the substitution of glycine by tryptophan (G34W) [15,16]. *H3-3A* is a histone variant encoding histone H3.3. H3.3 has an essential function in maintaining genome integrity in development and the cell cycle incorporated in chromatin. Mutations in *H3-3A* are also associated with various tumors aside from GCTB, including pediatric glioblastoma (K27M) and pediatric diffuse pontine glioma (K27M) [17,18]. In addition, chondroblastoma has a point mutation at the position of *H3F3B* (K36M), also encoding H3.3 [15,19]. Some MGCTs have an *H3-3A* G34W mutation, while others do not. Yoshida et al. demonstrated that an *H3-3A* G34W-negative component had an *H3-3A* copy-number deletion, whereas an *H3-3A* G34W-positive component had an intact *H3-3A* copy number; a subset of MGCTs had no *H3-3A* mutation [20]. Ishihara et al. also reported that *TP53* mutations may play a role in the malignant transformation of GCTB through interactions with dysfunction of histone methylation as evidenced by H3K27me3 loss [21]. However, the genetic mechanisms underlying the malignant transformation of GCTB are not clearly understood.

Thus, this study aimed to investigate the genetic changes throughout the course of treatment in MGCT. Moreover, we established a patient-derived organoid and organoid-derived xenograft (ODX) model from the MGCT and genetically defined that the established organoid line was a malignant transformed GCTB.

2. Materials and methods

2.1. Patient (OICI-MGCT-0876)

A 41-year-old Japanese man experienced a painful left knee 3 months before his presentation to our institute. Magnetic resonance imaging (MRI) revealed a bone tumor in the left distal femur, and he was referred to our hospital. The patient underwent lesion curettage and artificial bone grafting, and pathological examination revealed that the tumor was a GCTB (Fig. 1A, B and Fig. 2A, B). At the 10th year of follow-up, radiography revealed a relapse, and denosumab therapy was started. MRI at 1 year and 2 months after treatment initiation showed that the tumor had hardened, and thus, denosumab treatment was terminated. However, MRI at 2 years and 6 months after treatment termination showed recurrence. Denosumab was started again, and lesion curettage

and bone cement filling were performed 3 months later (Fig. 1A and C). Immunohistochemistry showed partial H3.3 G34W positivity, but microscopic examination revealed proliferating nests of atypical cells with pleomorphism (Fig. 2A and B).

Meanwhile, malignant cells tested negative for H3.3 G34W. Chemotherapy with doxorubicin, cisplatin, and a high dose of ifosfamide, which is a regimen against osteosarcoma [22], was administered. After four courses of chemotherapy, preoperative MRI showed a marked increase in tumor size and extraosseous extension. The patient underwent surgical resection with wide margins and arthroplasty, and we developed MGCT organoids from tumor samples (T3) (Fig. 1A and D). Microscopic examination revealed no evidence of a conventional GCTB image, and 60% of tumor cells were necrotic. Immunohistochemical analysis indicated negative results for H3.3 G34W (Fig. 2A and B). One month later, computed tomography (CT) revealed multiple distant metastases in the left inguinal region, liver, and lungs (Fig. 1A and E). The patient was treated with a combination of gemcitabine and docetaxel, but metastases in the liver and lungs increased in size. The tumor also did not respond to pazopanib treatment. The patient died of the disease 1 year after the diagnosis of MGCT.

2.2. Culture medium

The organoid culture medium was used as previously described [23]. Briefly, the basal medium consisted of Advanced Dulbecco's Modified Eagle's medium (DMEM)/F12 (Thermo Fisher Scientific) supplemented with HEPES (10 mM, Thermo Fisher Scientific), GlutaMAX (1x, Thermo Fisher Scientific), and penicillin–streptomycin-glutamine (1x, Thermo Fisher Scientific). The organoid culture medium consisted of basal medium supplemented with nicotinamide (10 mM, Sigma-Aldrich, St. Louis, MO, USA), N-acetylcysteine (1 mM, Wako), A-83-01 (500 nM, Wako), B-27 (1x, Gibco), recombinant human EGF (50 ng/mL, Sigma), gastrin I human (10 nM, Peprotech), recombinant human Noggin (100 ng/mL, Peprotech), recombinant human R-spondin 1 protein (500 ng/mL, R&D Systems), SB-202190 (10 µM, ChemScene), and 10% Afamin/Wnt3a CM (MBL).

2.3. Air-liquid interface organoid cultures

Primary MGCTs were obtained from the remaining surgically resected tissue (100–500 mg) as previously described [23]. Briefly, after four washes of the tumor tissues with ice-cold phosphate-buffered saline, the cells were minced with sterilized scissors and placed on a 60-mm dish for 15 min at room temperature (25 °C). The collected cells were suspended in DMEM (GIBCO, Grand Island, NY, USA) and incubated with 50 µg/ml of Liberase TH (Sigma-Aldrich) for 15 min at 37 °C. The supernatant was discarded, and the cells were incubated in 5 mL fetal bovine serum (Sigma) at 37℃ for 15 min to inactivate Liberase TH. The cells were suspended in 40 mL DMEM and passed through a 1000-µm cell strainer (pluriStrainer, pluriSelect Life Science UG & Co.KG) to remove debris.

After washing with the basal medium, the prepared cells (5×10^5-1×10^6) were suspended in the upper layer of the prepared collagen, and an organoid culture medium (1.5 mL) was added. The organoids were cultured at 37 °C in 95% air, 5% CO_2, and 100% humidity. The organoid culture medium was changed every 3 days. The collagen gel matrix (Cellmatrix type I-A, Nitta Gelatin Inc.) and culture dish were prepared according to the protocol of the organoid culture procedure as previously described [23]. After transferring the upper and bottom layers of collagen with organoids and mincing them, organoid culture was performed in the same manner as that for primary air–liquid interface ALI organoid cultures mentioned above. The minced organoids obtained during the passage were frozen in Stem Cell Banker (Amsbio ZENOAQ, 11890) and stored in a −80℃ freezer until use. When we thawed the stored organoid for use, their viability was about 60–80%.
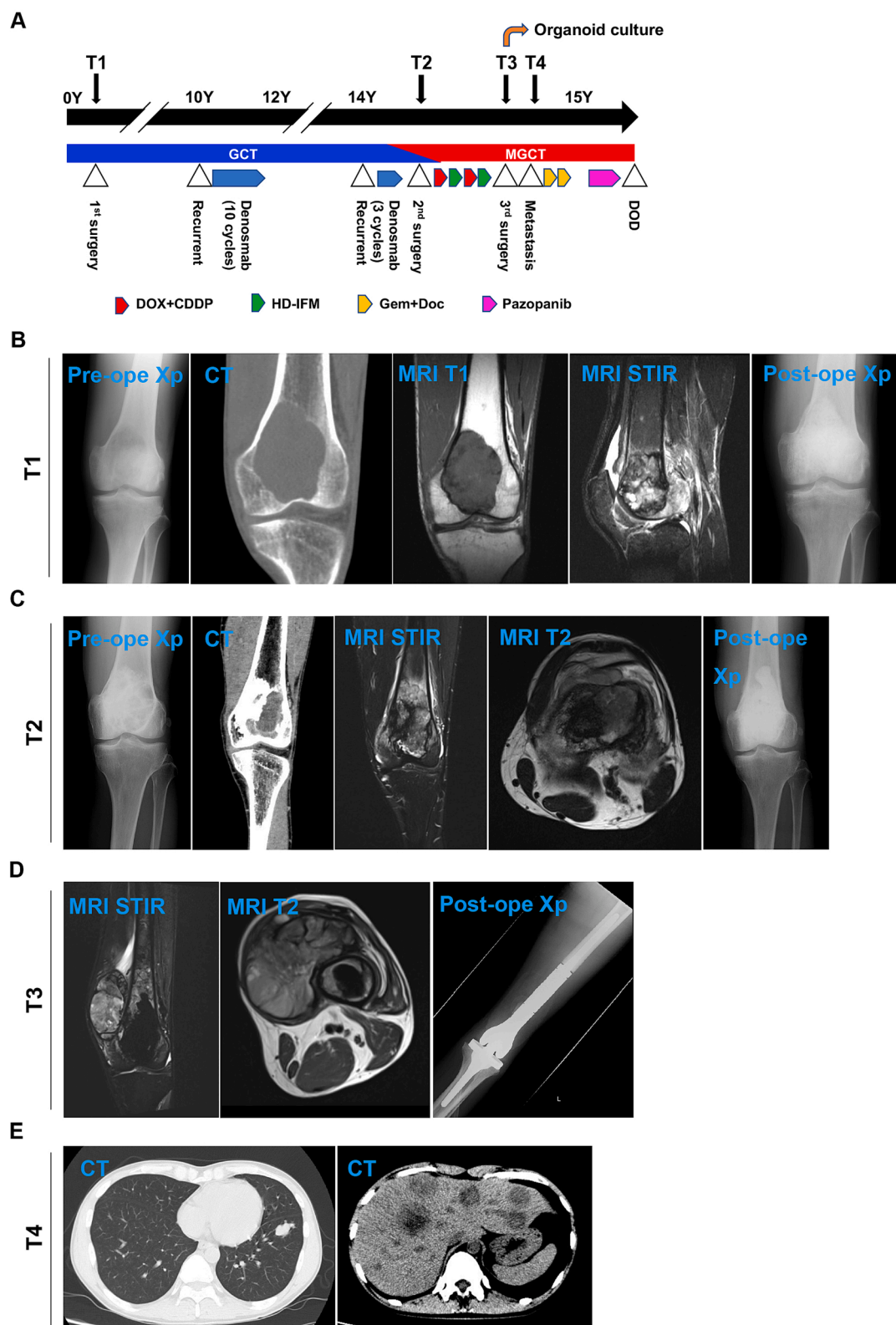
Fig. 1. MGCT in the left thigh of a 41-year-old man. (A) Clinical course. The treatment period is indicated with the black arrow; change in pathological diagnosis, blue and red bars. The white triangle shows the various clinical events, including surgery, progression of disease, and outcome. The colored pentagon indicates chemotherapies. DOX; doxorubicin, CDDP; cisplatin, HD-IFM; high-dose ifosfamide, Gem; gemcitabine, Doc; docetaxel. The organoids were established from the sample of 3rd surgery (T3). (B–E) Clinical images, including X-ray photograph (Xp), magnetic resonance imaging (MRI), and computed tomography (CT) at each time point. T1–4 indicates the time points 1–4, as shown in Fig. 1B–E and Fig. 2A–B. (For interpretation of the references to colour in this figure legend, the reader is referred to the web version of this article.)

2.4. Establishment of novel patient-derived organoid and ODX from an MGCT

After several serial passages with ALI organoid cultures, the cultured cells were xenografted into 6-week-old NOD-scid IL2Rgnull mice. The developed tumor was resected from the mouse, and the same tissue preparation steps, as described above, were performed. The ALI organoid culture was repeated for serial passages and xenografts in the NOD-scid IL2Rgnull mice. When the tumor developed, patient-derived organoids and ODX were established using the MGCTs. Mouse experiments were performed as previously described [23].

2.5. RNA and DNA isolation

Total RNA was extracted using the RNeasy Plus Universal Mini Kit (Qiagen) and RNeasy Mini Kit (Qiagen) according to the manufacturer's protocol. The purity was determined to be A260/A280 ratio above 2.0 for RNA. Total DNA from the original MGCT and the developed tumor was extracted using the DNeasy Blood & Tissue Kit (Qiagen) according to the manufacturer's protocol. The total DNA from the formalin-fixed paraffin-embedded (FFPE) tissue samples was extracted using the QIAamp DNA FFPE tissue kit (QIAGEN, Hilden, Germany) according to the manufacturer's protocol.
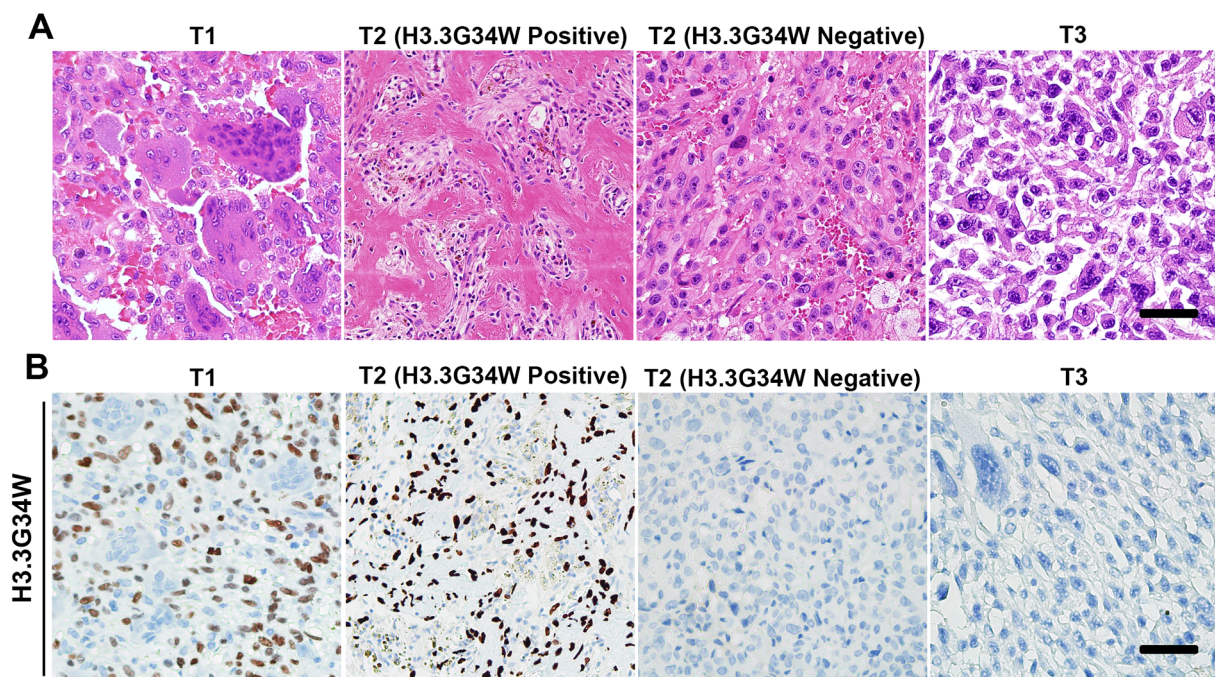
2.6. Immunohistochemistry

Immunohistochemical studies were performed to clarify whether the phenotypes of the cultured organoids and the developed tumors matched those of the original tumors. The tumor and organoid specimens were fixed in 10% neutral buffered formalin, embedded in paraffin, sectioned into 4-μm thickness, and stained with hematoxylin and eosin. Paraffin-embedded sections were deparaffinized and dehydrated. The antigens were retrieved at 95 °C for 15 min in pH 6.0 citric acid buffer. After blocking endogenous peroxidase activity for 15 min with 3% hydrogen peroxide solution, the sections were incubated for 1 h with 2.5% normal horse serum at room temperature to prevent nonspecific binding.

Next, the sections were incubated overnight with a primary antibody in a blocking solution at 4 °C. After washing with phosphate-buffered saline, the slides were incubated with ImmPress horseradish peroxidase anti-rabbit immunoglobulin G peroxidase polymer secondary (Vector Laboratories) for 30 min, followed by DAB staining (Peroxidase Stain DAB Kit, Nacalai) until the appropriate stain intensity developed (1–2 min). The slides were washed and counterstained with Gill No. 3 hematoxylin (Sigma-Aldrich) for 45 s. As a negative control, staining was performed in the absence of primary antibodies. The histological analyses were performed by a pathologist at our institute. Primary antibodies against Anti-Histone H3.3 (mutated G34W, rabbit monoclonal, clone RM307, dilution 1:2000; RevMAb Biosciences) were used.

2.7. Organoid proliferation assay

An organoid proliferation assay was performed as previously described [23]. Briefly, cell suspensions from cultured MGCT organoids were prepared according to ALI organoid-culture procedures. The collagen gel matrix was prepared according to an organoid-culture procedure. Millicell culture plate inserts (PICM 01250, Millicell-CM, Millipore) were placed in a 24-well culture plate (Thermo Fisher Scientific) to prepare the culture dish. To form the bottom layer, 150 μL of prepared reconstituted collagen solution was added to the inserts under sterile conditions. At 30 min after incubation for solidification at 37 °C, the prepared cells (1×10^5 cells/well) were counted and collected. They were then cultured in the upper layer of the prepared 150 μL of collagen with 200 μL of organoid culture medium at 37 °C with 95% air, 5% CO_2, and 100% humidity for 72 h.

3-(4,5-Dimethyl-2-thiazolyl)-2,5-diphenyltetrazolium bromide (MTT) assays were used to detect live organoids 72 h after treatment with doxorubicin (Wako) at concentrations of 0.15–1.5 μM or everolimus (Wako) at concentrations of 10–1000 nM. Everolimus is a clinically used mammalian target of rapamycin (mTOR) inhibitor and was selected in the current study from among targets based on genomic analysis in the MGCT case. Live organoids were detected by adding 100 μL of 5 mg/mL MTT solution in phosphate-buffered saline and incubating for 4 h. In this method, only live organoids could be detected as

Fig. 2. Histological appearance of the original tumor. (A) Hematoxylin & eosin staining of original tumors at each time point. (B) Immunohistochemical reactivity against H3.3 G34W antibody in the original tumor at each time point. Scale bar: 100 μm. In T2, H3.3 G34W positive and negative lesions were separately demonstrated.

blue spots, and the spot areas were counted using ImageJ according to the manufacturer's protocol.

Cell viability was also evaluated with the CellTiter-Glo® 3D according to the manufacturer's protocol for experiments of growth curve and drug treatment of everolimus.

2.8. RNAseq analysis

The total RNA was sent to Seibutsu Giken Inc. (Kanagawa, Japan) for next-generation sequencing. RNA sample concentrations were measured using a Quantus Fluorometer and Quanti Fluor RNA System (Promega). RNA quality was checked using a 5200 Fragment Analyzer System and Agilent HS RNA Kit (Agilent Technologies). The next-generation sequencing library was prepared using the MGIEasy RNA Directional Library Prep Set (MGI Tech Co., Ltd.), according to the manufacturer's protocol. Library concentrations were measured using the Synergy LX and Quanti Fluor dsDNA systems, while library quality was checked using a Fragment Analyzer and dsDNA915ReagentKit (Advanced Analytical Technologies). Circular DNA was prepared from the library using the MGIEasy Circularization Kit (MGI Tech Co., Ltd.).

DNA nanoballs (DNB) were made with DNBSEQG 400 RS high-throughput sequencing kit (MGI Tech Co Ltd) according to the manufacturer's protocol. Sequencing was performed using DNBSEQ-G400 for at least 2×100 bp read. Adapters and primers from the delivered FASTQ files were removed using Cutadapt (ver. 1.9.1). Short-read sequences (under 20) and low-quality score reads (<40) were removed using a sickle (ver. 1.33). HISAT2 (ver. 2.2.1) was used to read the alignment and map the GRCh38 reference genomes. After reading and writing the alignment data in SAM and BAM formats using SAMtools, the data were sorted and indexed. Read counts per gene were obtained using featureCounts (ver. 2.0.0). The relative expression level of each gene was normalized to the reads per kilobase million and transcripts per million. The genetic characteristics and transcriptome profiles were analyzed and visualized using iDEP and RaNA-seq [24,25].

2.9. Whole-exome sequencing analysis

The total DNA of the tumor samples and matched normal tissue was sent to Rhelixa (Tokyo, Japan) for whole-exome sequencing. The concentrations and quality of the DNA samples were measured using Qubit and gel electrophoresis. Sequencing was performed using target capture with an Agilent SureSelect V6 58 M. Raw sequence data were generated using Illumina NovaSeq 6000 sequencers. Quality checks of the library were performed using the FastQC software. After trimming the sequencing data with Trimmomatic software (ILLUMINACLIP 2:30:10), sequencing data were mapped to the reference genome using BWA software. Deduplication reads were excluded, and an interval list defining the area of the exome kit target was created using Picard software. Base scores of the generated BAM files were corrected, and small polymorphisms were extracted using GATK (BaseRecalibrator and ApplyBSQR).

Somatic mutations between tumor samples and paired normal tissues were identified using GATK (Mutect2). Information on the obtained single-nucleotide variant, including genotype and amino acid, was annotated and integrated into the variant call format file. The variant allele frequency (VAF) was calculated using the following formula: alteration reads / (alteration reads + reference reads). The candidate mutations in a sample were listed according to the following criteria: (i) number of detections among the samples ≥ 2, (ii) ≥ 50 variant reads in the sample, (iii) VAF in the sample ≥ 0.1, and (iv) putative impact annotated as high or moderate with mutations in the protein-coding region. Copy number variation between normal tissue and tumor samples was analyzed using the CNVkit.

2.10. Statistical analysis

Data were analyzed using Student's *t*-test. All statistical analyses were performed using Excel (Microsoft, Inc, Redmond, Washington). Statistical significance was set at P < 0.05.

3. Results

3.1. Establishment of a novel organoid line from human MGCT (OICI-MGCT-0876)

The organoids grew steadily over time during serial passages and their viability increased by approximately 2.5-fold in 72 h (Fig. 3A and B). The size of the MGCT organoids increased in a short period, the organoid morphology was distorted, and dendritic morphology growing from the organoid surface was observed (Fig. 3C). On culturing for >2 weeks, some organoids aggregated and could not be easily broken during the pipetting phase of the passage procedures, indicating strong cell–cell adhesion in the organoids (Fig. 3D). MGCT organoids were repeatedly xenografted in mice, and tumors developed within 30–60 days. These tumors demonstrated a pleomorphic histological appearance resembling that of the original tumor under hematoxylin and eosin staining (Fig. 3A and E). Immunohistochemical analysis of the xenografted tumor was negative for H3.3 G34W (Fig. 3E). This indicated that OICI-MGCT-0876 had high tumorigenesis and retained its original characteristics.

3.2. Genetic changes and characteristics of OICI-MGCT-0876

Fifteen of 26 (57.7%) mutations in the selected genes, including oncogenic mutations of *TP53* and *TSC2*, were more enriched in MGCT than in GCTB (Fig. 4A and Table S1). Almost all of these mutations, including *TP53* and *TSC2*, were detected in the established MGCT organoids, indicating that the characteristics of genomic alterations were preserved to some extent in these organoids (Fig. 4A). Copy number alterations were more frequent in MGCT than in GCTB, indicating that MGCT had higher genomic instability (Fig. 4B). In addition, the *H3-3A* mutation was detected in GCTB but not in MGCT and ODX (Fig. 4A). Copy number analysis also indicated that the chromosomal region, including *H3-3A*, was lost (Fig. 4B). The *H3-3A* mutation (G34W) was absent in MGCT through malignant transformation because the mutated chromosomal region, including *H3-3A*, might be deleted owing to genomic instability (Fig. 4C).

3.3. Transcriptome profiling in OICI-MGCT-0876

The heatmap, correlation matrix, scatter plot, and principal component analysis of the gene expression of each sample are shown in Fig. 5A-C, Supplemental Figs. S1–S3, and Table S2. The gene-expression profiles of the normal tissue did not correlate with those of the original GCTB, MGCT, PDO or ODX (Supplementary Fig. S1). The gene profiles of GCTB showed moderate correlations with those of MGCT, PDO and ODX. Meanwhile, the gene profiles of MGCT and ODX were strongly correlated. These results suggested that the gene expression signatures of OICI-MGCT-0876 tumors were almost identical to those of primary MGCT tumors. In addition, gene expression signatures were enriched through the malignant transformation from GCTB to MGCT. Transcriptome analysis showed that 4466 and 641, 6746 and 595, and 5336 and 715 genes were upregulated and downregulated in MGCT, ODXs and PDOs, respectively, compared to the normal tissue at fold changes >2 (Fig. 5D and Tables S3–S5).

CD44 is involved in cancer stem cells and plays a role in cancer development and progression [26,27]. *TWIST* is involved in metastasis, chemoresistance, and epithelial–mesenchymal transition [28,29]. *CD44* and *TWIST* expression was markedly high in tumors and ODX (Fig. 5D). Enrichment analysis showed that the mTOR and *TP53* pathways were
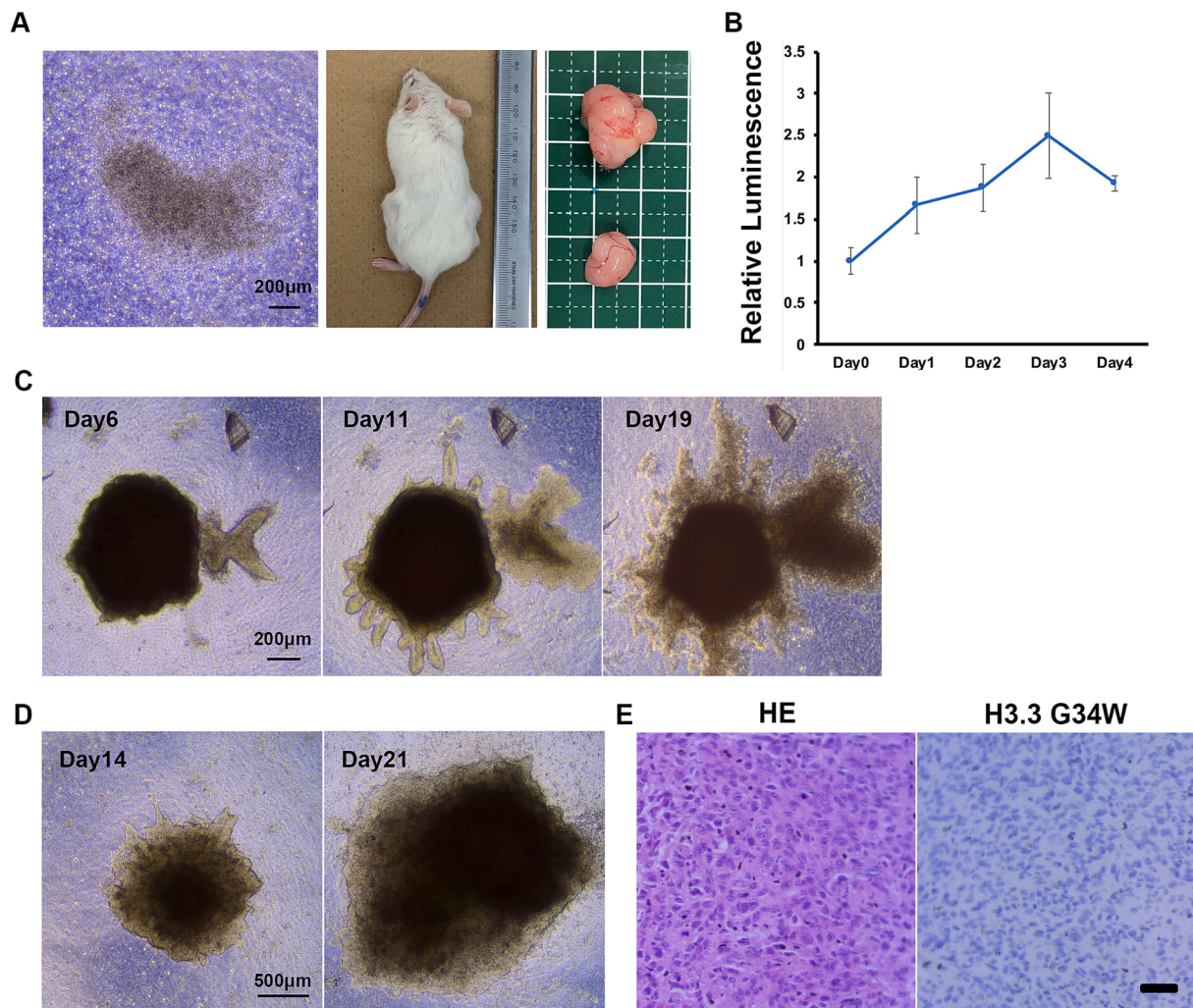
Fig. 3. Establishment of PDO and ODX models of OICI-MGCT-0876. (A) Morphology of OICI-MGCT-0876 organoids under ALI organoid culture by phase-contrast microscopy (left). Developed tumors on NSG mice of ODX from PDO of OICI-MGCT-0876 (middle and right). (B) Growth curve of PDO from day 0 to day 4. Cell viability was demonstrated with relative luminescence. (C) Images of growing organoid of OICI-MGCT-0876 at days 6, 11, and 19. Scale bar: 200 μm. (D) Organoid images of OICI-MGCT-0876 in long periods of culture. Scale bar: 500 μm. (E) Hematoxylin & eosin staining (left) and immunohistochemical reactivity against H3.3 G34W antibody in xenografted tumor of OICI-MGCT-0876. Scale bar: 100 μm.

activated in MGCT and ODX (Supplementary Fig. S4A). The results of Kmeans enrichment analyses for functional and ontological characterization of genes are shown in Supplementary Fig. S4B and Tables S6 and S7. Gene expression was clustered into four groups, and cluster B was enriched in both the original MGCT, ODXs and PODs. In this cluster, 283 genes and 15 biological pathways were identified, including the TP53 signaling pathway (5 genes) and the PI3K-Akt signaling pathway (14 genes). In addition, almost osteoblastic and osteoclastic markers were high in GCTB but not in MGCT, ODXs and PDOs (Supplementary Fig. S5).

With respect to response to chemotherapy and genome-based targeted therapy for MGCT, organoid proliferation assay in OICI-MGCT-0876 indicated that doxorubicin showed little antitumor efficacy for MGCT, despite it being the first-line drug for sarcomas. In addition, 0.15–1.5 μM doxorubicin and 10–1000 nM everolimus did not effectively suppress the organoid growth of OICI-MGCT-0876 (Supplementary Fig. S4C). We also confirmed the organoids showed the resistance for the treatment of everolimus with CellTiter-Glo® 3D whereas those organoids were almost dead with cell lysis buffer treatment as positive control (Supplementary Fig. S4D). This demonstrated that OICI-MGCT-0876 was resistant to doxorubicin and everolimus.

4. Discussion

The present study established and reported MGCT organoids from a typical case of MGCT and treated them with genome-based treatment. The organoids showed strong chemoresistance and high *CD44* and *TWIST* expressions. *CD44* and *TWIST* expressions are strongly correlated with chemoresistance in various cancers [26–29], which could explain the current findings. To the best of our knowledge, the present study is the first to establish MGCT organoids from a typical case of MGCT.

CD44 is negatively regulated by *TP53* binding to a noncanonical TP53-binding sequence in the *CD44* promoter. Similar to previous reports [26,27], our MGCT case showed high mRNA expression of *CD44* when there was a *p53* mutation. *TWIST* is a negative regulator of the TP53-mediated response to cellular stress that acts by modulating both ARF expression and p53 post-translational modifications, such as phosphorylation and acetylation [28]. Furthermore, *CD44* promotes c-Src-mediated *TWIST* transcriptional activation [30]. In OICI-MGCT-0876, these genes cooperate in various ways to exhibit malignant potential. We also demonstrated that the *H3-3A* mutation was lost during malignant transformation through loss of heterozygosity (LOH) with copy number loss, supporting a previous finding [20] (Fig. 4C). Although such genetic diversity might occur owing to genomic
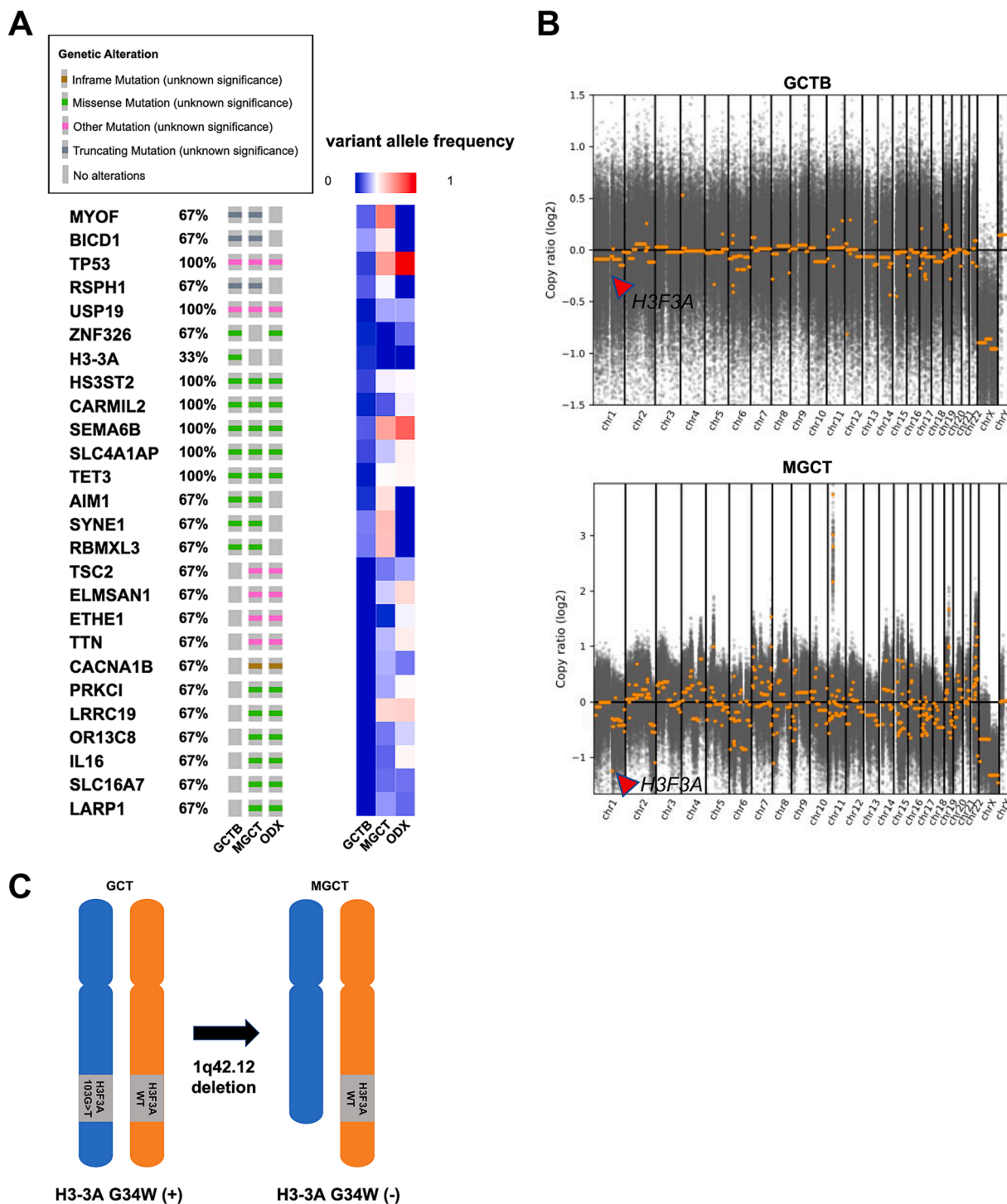
Fig. 4. Genetic changes and characteristics in malignant transformation from GCTB to MGCT and OICI-MGCT-0876. (A) Somatic mutations, including single-nucleotide variants (SNVs) and short insertions/deletions (INDELs) (Left panel). Variant allele frequency of each mutation is visualized using a heatmap (Right panel). (B) Copy number variations in tumors of GCTB and MGCT. *H3-3A*, located at chromosome 1 is indicated with red triangles. (C) *H3-3A* mutation status in the present MGCT. The mutation is lost during malignant transformation through loss of heterozygosity with copy number losses (CNL-LOH). (For interpretation of the references to colour in this figure legend, the reader is referred to the web version of this article.)

instability, the prognostic impact of the *H3-3A* gene in MGCT is unclear. More than 90% of GCTB cases have an *H3-3A* G34W mutation, suggesting that the mutation could be the causative gene for tumorigenesis. However, previous studies indicated that *H3-3A* may not play an oncogenic role in MGCT. This needs to be clarified through further accumulation of cases and clarification of the underlying mechanism of H3.3 functions.

Denosumab, a humanized monoclonal antibody on RANKL, has been proven to be beneficial for GCTB [31,32]. Denosumab was administered to the patient in this study. Although studies reporting the risk of malignant transformation in GCTB have increased, the hypothesis remains controversial. The largest clinical trial of denosumab against GCTB reported no increase in the risk of malignant transformation of GCTB (1%) and found no biological evidence to support a causal association
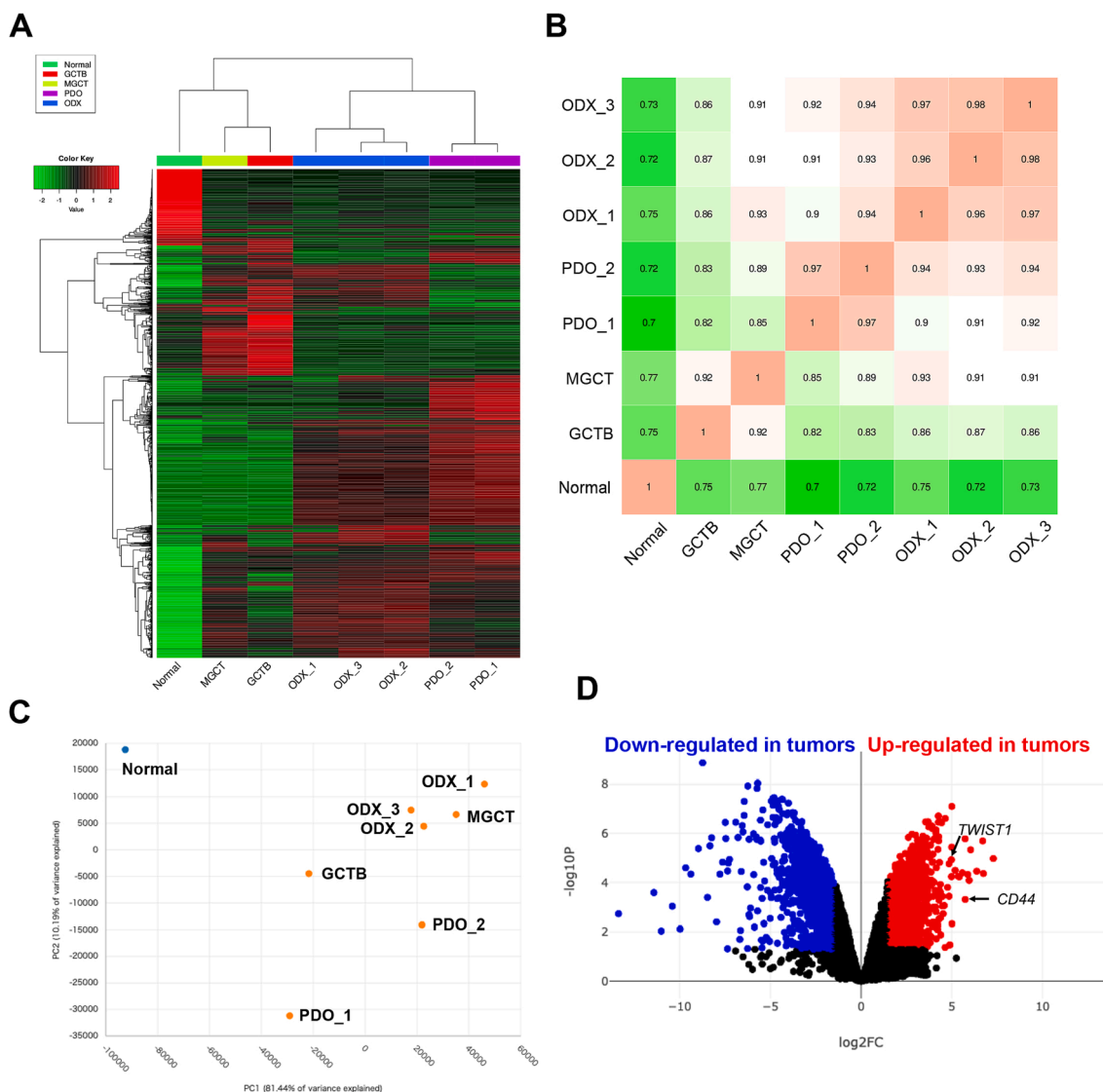
Fig. 5. Transcriptome analysis of OICI-MGCT-0876. (A) Heatmap showing the gene expression profiling (1200 genes) of normal tissue (Normal), original tumors (GCTB and MGCT), OICI-MGCT-0876 tumors developed in NSG mice (ODXs), and PDOs. (B) Correlation matrix between samples using the top 75% genes. (C) Principal component analysis (PCA) between normal and tumor tissue samples. (D) Volcano plots of the up- and downregulated genes in ODX and GCTB and MGCT compared to normal tissues. The plot displayed the log2-fold changes and statistical significance of each gene calculated by performing a differential gene expression analysis. Every point in the plot represents a gene. Red points indicate significantly up-regulated genes, blue points indicate down-regulated genes. And points of *CD44* and *TWIST1* were indicated. (For interpretation of the references to colour in this figure legend, the reader is referred to the web version of this article.)

between malignancy and denosumab treatment [33]. Although denosumab was used to treat the GCTB patient in this study for more than 10 cycles, and it took over 2 years of treatment with the drug for malignant transformation to occur, we could not establish the definite cause of the malignant transformation. The patient was first diagnosed with MGCT at the second surgery, and we found both GCTB and MGCT regions by histological analysis. In the third surgery, performed 4 months after the second surgery, only malignant transformed cells were found. This indicated that malignant cells rapidly became dominant in the MGCT. Therefore, malignant transformation may have occurred shortly and rapidly before the second surgery. Another possibility is that malignant transformation occurred a long time ago, but the malignant cells remained dormant. Accordingly, we investigated the genetic status, including oncogenic mutations, such as *TP53*, of GCTB at the first surgery. However, we could not obtain high-quality DNA from the paraffin-embedded tissue samples. Further research is required for these investigations.

The present study had some limitations. First, we established a

sarcoma organoid line of MGCT using the ALI organoid culture method. However, it is unclear whether the ALI organoid culture method is suitable for MGCT cells, although the established OICI-MGCT-0876 showed representative characteristics of MGCT. Second, this study was conducted at a single institution. Therefore, it is possible that unintentional bias in the experimental procedures was not fully eliminated, and further investigation with a larger number of sarcoma samples is required.

In conclusion, we presented a novel organoid model of MGCT that was genetically confirmed to be a malignant transformed tumor. Our organoid model could be a good model to elucidate the molecular pathogenesis of MGCT and develop novel treatment modalities.

5. Ethics Approval/Consent to Participate

The experiments were performed in accordance with the guidelines of the Institutional Review Board for Clinical Research after obtaining informed consent from the patient (approval number; 1710059174-6).

All animal experiments were approved (approval number; 20111910) by the Institutional Committee of Animal Care of the Osaka International Cancer Institute, and all animals were euthanized with diethyl ether at the end of the experiments.

6. Author Contribution Statement

RS, TW, YY, SS, Ken-ici Y, and ST designed the study. RS and TW collected, interpreted, and analyzed the data. TW performed the statistical analyses. RS and TW wrote the manuscript. TW, Keiichi Y, and YM performed the *in vitro* and mouse experiments. HT, TW, YI, SN, TY, SK, and ST treated patients. Ken-ici Y performed the pathological diagnosis and experiments. All authors revised the manuscript critically for important intellectual content and read and approved the final manuscript.

7. Data Availability Statement

All data generated or analyzed during this study are included in this published article and its supplementary information files. The raw sequences data have been deposited in the DNA Data Bank of Japan (DDBJ) with accession number BioProject: PSUB020193.

8. Funding Statement

CRediT authorship contribution statement

Rie Suzuki: Conceptualization, Methodology, Writing – original draft. **Toru Wakamatsu:** Conceptualization, Methodology, Writing – original draft, Visualization, Funding acquisition. **Keiichi Yoshida:** Investigation, Methodology. **Yukiko Matsuoka:** Investigation, Methodology. **Haruna Takami:** Resources, Supervision. **Sho Nakai:** Resources, Supervision. **Hironari Tamiya:** Resources, Supervision. **Shigeki Kakunaga:** Resources, Supervision. **Toshinari Yagi:** Resources, Supervision. **Ken-ichi Yoshida:** Conceptualization, Methodology, Investigation. **Yoshinori Imura:** Supervision. **Yoshihiro Yui:** Supervision. **Satoru Sasagawa:** Supervision. **Satoshi Takenaka:** Resources, Supervision.

Declaration of Competing Interest

The authors declare that they have no known competing financial interests or personal relationships that could have appeared to influence the work reported in this paper.

Acknowledgements

Appendix A. Supplementary data

Supplementary data to this article can be found online at https://doi.org/10.1016/j.jbo.2023.100486.

References

[1] J.J. Eckardt, T.J. Grogan, Giant cell tumor of bone, Clin. Orthop. Relat. Res. 204 (1986) 45–58.
[2] D.C. Dahlin, R.E. Cupps, E.W. Johnson, Giant-cell tumor: A study of 195 cases, Cancer 25 (1970) 1061–1070, https://doi.org/10.1002/1097-0142(197005)25:5%3C1061::aid-cncr2820250509%3E3.0.co;2-e.
[3] H.S. Schwartz, Giant cell tumor of bone, Compr. Ther. 19 (1993) 64–68.
[4] B. Czerniak, Giant cell lesions, in: B. Czerniak (Ed.), Dorfman and Czerniak's Bone Tumors, 2nd ed., Elsevier, Philadelphia, 2016, pp. 692–759.
[5] L. Gong, W. Liu, X. Sun, C. Sajdik, X. Tian, X. Niu, et al., Histological and clinical characteristics of malignant giant cell tumors of the bone, Virchows Arch. 460 (2012) 327–334, https://doi.org/10.1007/s00428-012-1198-y.
[6] E. Palmerini, P. Picci, P. Reichardt, G. Downey, Malignancy in giant cell tumor of bone: A review of the literature, Technol Cancer Res Treat. 18 (2019) 1533033819840000. https://doi.org/10.1177/1533033819840000 .
[7] W. Liu, C.M. Chan, L. Gong, M.M. Bui, G. Han, G.D. Letson, et al., Malignancy in giant cell tumors of bone in the extremities, J. Bone Oncol. 26 (2021), 100334, https://doi.org/10.1016/j.jbo.2020.100334.
[8] F. Bertoni, P. Bacchini, E.L. Staals, Malignancy in giant cell tumor of bone, Cancer 97 (2003) 2520–2529, https://doi.org/10.1016/j.jbo.2020.100334.
[9] P. Anract, G. De Pinieux, P. Cottias, P. Pouillart, M. Forest, B. Tomeno, Malignant giant cell tumors of the bone. Clinicopathological types and prognosis: a review of 29 cases, Int. Orthop. 22 (1998) 19–26.
[10] X. Zhu, R. Huang, P. Hu, P. Yan, S. Zhai, J. Zhang, J. Zhuang, H. Yin, T. Meng, D. Yang, Z. Huang, Prognostic factors for survival in patients with malignant giant cell tumor of bone: A risk nomogram analysis based on the population, Med. Sci. Monit. 27 (2021) e929154.
[11] K.K. Unni, Diagnosis of malignant giant cell tumors, Pathol Case Rev. 6 (2001) 33–37.
[12] K. Skubitz, Giant cell tumor of bone: current treatment options, Curr. Treat. Options Oncol. 15 (2014) 507–518, https://doi.org/10.1007/s11864-014-0289-1.
[13] I. Kato, M. Furuya, K. Matsuo, Y. Kawabata, R. Tanaka, K. Ohashi, Giant cell tumors of bone treated with denosumab: Histological, immunohistochemical, and H3F3A mutation analyses, Histopathology 72 (2018) 914–922, https://doi.org/10.1111/his.13448.
[14] M. Hasenfratz, K. Mellert, R. Marienfeld, A. von Baer, M. Schultheiss, P.D. Roitman, *et al.*, Profiling of three H3F3A-mutated and denosumab-treated giant cell tumors of the bone points to diverging pathways during progression and malignant transformation, Sci Rep. 11 (2021) 5709. https://doi.org/10.1038%2Fs41598-021-85319-x.
[15] S. Behjati, P.S. Tarpey, N. Presneau, S. Scheipl, N. Pillay, P. Van Loo, et al., Distinct H3F3A and H3F3B driver mutations define chondroblastoma and giant cell bone tumors, Nat. Genet. 45 (2013) 1479–1482, https://doi.org/10.1038/ng.2814.
[16] F. Amary, F. Berisha, H. Ye, M. Gupta, A. Gutteridge, D. Baumhoer, R. Gibbons, R. Tirabosco, P. O'Donnell, A.M. Flanagan, H3F3A (histone 3.3) G34W immunohistochemistry: a reliable marker defining benign and malignant giant cell tumors of bone, Am. J. Surg. Pathol. 41 (8) (2017) 1059–1068.
[17] L. Bjerke, A. Mackay, M. Nandhabalan, A. Burford, A. Jury, S. Popov, et al., Histone H3.3. mutations drive pediatric glioblastoma through the upregulation of MYCN, Cancer Discov. 3 (2013) 512–519, https://doi.org/10.1158/2159-8290.cd-12-0426.
[18] K. Aihara, A. Mukasa, K. Gotoh, K. Saito, G. Nagae, S. Tsuji, K. Tatsuno, S. Yamamoto, S. Takayanagi, Y. Narita, S. Shibui, H. Aburatani, N. Saito, H3F3A K27M mutations in thalamic gliomas from young adult patients, Neuro Oncol. 16 (1) (2014) 140–146.
[19] M.F. Amary, F. Berisha, R. Mozela, R. Gibbons, A. Guttridge, P. O'Donnell, et al., The H3F3 K36M mutant antibody is a sensitive and specific marker for chondroblastoma diagnosis, Histopathology 69 (2016) 121–127, https://doi.org/10.1111/his.12945.
[20] K.I. Yoshida, Y. Nakano, M. Honda-Kitahara, S. Wakai, T. Motoi, K. Ogura, et al., Absence of H3F3A mutation in a subset of malignant giant cell tumors of the bone, Mod. Pathol. 32 (2019) 1751–1761, https://doi.org/10.1038/s41379-019-0318-5.
[21] S. Ishihara, H. Yamamoto, T. Iwasaki, Y.u. Toda, T. Yamamoto, M. Yoshimoto, Y. Ito, Y. Susuki, K. Kawaguchi, I. Kinoshita, Y. Yamada, K. Kohashi, T. Fujiwara, N. Setsu, M. Endo, Y. Matsumoto, Y. Kakuda, Y. Nakashima, Y. Oda, Histological and immunohistochemical features and genetic alterations in the malignant progression of giant cell tumor of bone: a possible association with TP53 mutation and loss of H3K27 trimethylation, Mod. Pathol. 35 (5) (2022) 640–648.
[22] D. Carrle, S.S. Bielack, Current strategies of chemotherapy in osteosarcoma, Int Orthop. 30 (2006) 445–451. https://doi.org/10.1007%2Fs00264-006-0192-x.
[23] T. Wakamatsu, H. Ogawa, K. Yoshida, Y. Matsuoka, K. Shizuma, Y. Imura, et al., Establishment of organoids from human epithelioid sarcoma with–the liquid interface organoid culture, Front. Oncol. 12 (2022), 893592, https://doi.org/10.3389/fonc.2022.893592.
[24] S.X. Ge, E.W. Son, R. Yao, iDEP: an integrated web application for differential expression and pathway analysis of RNA-Seq data, BMC Bioinf. 19 (2018) 534, https://doi.org/10.1186/s12859-018-2486-6.
[25] C. Prieto, D. Barrios, RaNA-Seq: Interactive RNA-Seq analysis from FASTQ files for functional analysis, Bioinformatics 36 (2019) 1955–1956, https://doi.org/10.1093/bioinformatics/btz854.
[26] S. Godar, T.A. Ince, G.W. Bell, D. Feldser, J.L. Donaher, J. Bergh, et al., Growth-inhibitory and tumor-suppressive functions of p53 depend on the repression of CD44 expression, Cell 134 (2008) 62–73, https://doi.org/10.1016/j.cell.2008.06.006.
[27] C. Chen, S. Zhao, A. Karnad, J.W. Freeman, The biology and role of CD44 in cancer progression: therapeutic implications, J. Hematol. Oncol. 11 (2018) 64, https://doi.org/10.1186/s13045-018-0605-5.
[28] A. Puisieux, S. Valsesia-Wittmann, S. Ansieau, Twisting for survival and cancer progression, Br. J. Cancer. 94 (2006) 13–17. https://doi.org/10.1038%2Fsj.bjc.6602876.
[29] W.K. Kwok, M.-T. Ling, T.-W. Lee, T.C.M., Lau, C. Zhou, X. Zhang,, et al., Upregulation of TWIST in prostate cancer and its implications as a therapeutic

target, Cancer Res. 65 (2005) 5153–5162, https://doi.org/10.1158/0008-5472. can-04-3785.

[30] L.Y.W. Bourguignon, G. Wong, C. Earle, K. Krueger, C.C. Spevak, Hyaluronan-CD44 interaction promotes c-Src-mediated twist signaling, microRNA-10b expression, and RhoA/RhoC up-regulation, leading to Rho-kinase-associated cytoskeleton activation and breast tumor cell invasion, J. Biol. Chem. 285 (2010) 36721–36735, https://doi.org/10.1074/jbc.m110.162305.

[31] H. Li, J. Gao, Y. Gao, N. Lin, M. Zheng, Z. Ye, et al., Denosumab in giant cell tumor of bone: Current status and pitfalls, Front. Oncol. 10 (2020), 580605, https://doi.org/10.3389/fonc.2020.580605.

[32] A. Lipplaa, S. Dijkstra, H. Gelderblom, Challenges of denosumab in giant cell tumor of bone, and other giant cell-rich tumors of bone, Curr. Opin. Oncol. 31 (2019) 329–335, https://doi.org/10.1097/cco.0000000000000529.

[33] S. Chawla, R. Henshaw, L. Seeger, E. Choy, J.-Y. Blay, S. Ferrari, J. Kroep, R. Grimer, P. Reichardt, P. Rutkowski, S. Schuetze, K. Skubitz, A. Staddon, D. Thomas, Y.i. Qian, I. Jacobs, Safety and efficacy of denosumab for adults and skeletally mature adolescents with giant cell tumour of bone: Interim analysis of an open-label, parallel-group, phase 2 study, Lancet Oncol. 14 (9) (2013) 901–908.